immuno-isolated with a pan-p3-Alcα antibody. By semi-quantitative estimation with the mass spectrometric analysis, approximately 70% or more of the p3-Alcα species is p3-Alcα35 [7]. Furthermore, using an ELISA system with the pan-p3-Alcα antibody, which can detect all of the p3-Alcα species and quantify total amounts of p3-Alcα, we estimated a total of 5,000–15,000 pg/mL of p3-Alcα in the CSF of human subjects. The levels are comparable to the $A\beta_{40}$ levels, and increase in AD patients with a significant correlation to $A\beta_{40}$ levels in the CSF [22]. p3-Alcα is detectable in the plasma, but the total p3-Alcα content in the plasma is less than that detected in the CSF, and approximately 50–300 pg/mL of total p3-Alcα is quantified by the pan-p3-Alcα sELISA system [21]. Although the total plasma p3-Alcα levels also increase in AD patients, it remains unclear whether the p3-Alcα35 levels increase in AD patients.

In the present study, we analyzed levels of plasma p3-Alcα35, a major species of the p3-Alcα peptides generated from the cleavage of Alcα by γ-secretase, by using a newly established ELISA system with a C-terminal end-specific monoclonal antibody. First, we found that p3-Alcα35 is a major p3-Alcα species in the plasma, and we can estimate approximately 60% or more of total p3-Alcα species is p3-Alcα35 in the plasma, which is a comparable ratio to that of the CSF. We also found that the p3-Alcα35 levels in the plasma increased in subjects with a lower MMSE score in two of three of the cohorts, although the plasma levels appeared to increase in an age-dependent manner. In age-matched subjects, the p3-Alcα35 levels increased in AD patients of two of the cohorts. One cohort showed a significant increase in p3-Alcα35 levels in a CDR-dependent manner among age-matched subjects. Taken together, the plasma p3-Alcα35 levels showed an increase in subjects who appear to have cognitive impairment, as demonstrated by the total p3-Alcα levels [21, 23]. However, the increased magnitude of plasma p3-Alcα35 in AD was small compared to the total amount of p3-Alcα detected in our previous studies using the sELISA system with the polyclonal pan-p3-Alcα antibody [21, 23]. Therefore, we cannot rule out the possibility that the p3-Alcα35 specific monoclonal antibody may lack some component(s) of p3-Alcα that are greatly increased in the blood of AD patients.

Unfortunately, we could not detect a significant increase of p3-Alcα35 levels of AD patients in Cohort 3. This may be due to a cause of heterogeneity of sporadic AD patients. We previously suggested that causes of sporadic AD may be variable [22], and a recent publication for the different Aβ fibril formation in individual AD patients supports this idea [27]. Alternatively, in blood examination, the quantification of p3-Alcα35 alone may be difficult to classify AD patients clearly. Combination assay with another blood marker may be more effective for blood sample.

The age-matched AD subject population of CDR 1 and CDR 2 treated with donepezil showed lower plasma p3-Alcα35 values than the population without treatment. Although it remains unclear how donepezil lowers the level of p3-Alcα35 (and this is a result of limited number of subjects), the improvement of neuronal activity may contribute to the suppression of the increase in p3-Alcα35 levels, or facilitating the removal of p3-Alcα35. A more convincing study, such as a study to compare the levels of p3-Alcα35 in patients with AD before and after donepezil treatment, will be needed to confirm this effect. The plasma p3-Alcα35 levels can be reflected by the levels detected in the CSF of patients with cognitive impairment. If so, the level of plasma p3-Alcα35 may be an indicator of cognitive ability of aged subjects. Another peptide derived from γ-secretase cleavage of the AβPP-like protein 1 (APLP1) is also reported to reflect the amyloidogenic state of AβPP metabolism in the brain [17]. The concentration of this peptide in the CSF (4.5 nM) is comparable to the level of p3-Alcα in the CSF [22]; however, the concentration of the APLP1 peptide in the plasma has not been determined. Aβ and p3-Alcα are the main γ-secretase peptide products of the type I membrane proteins expressed largely in the brain that are detectable in the plasma. AβPP695 shows neuron-specific expression, while other isoforms such as AβPP770/751 are moderately expressed in non-neuronal tissues, including immunocompetent cells in the blood [10, 28, 29]. p3-Alcα is largely derived from the brain because Alcα expression is mostly observed in the brain [2], and increased plasma p3-Alcα levels are detected in Alcα-CTF transgenic mice with a neuron-specific promoter (unpublished observation). Moreover, it should be noted that AβPP and Alc express and colocalize largely in neurons, appear to have the same function as kinesin-1 cargo receptors, and are subject to similar proteolytic metabolism [2, 5, 7, 9]. Therefore, changes in the quality and quantity of the plasma p3-Alcα levels may provide a glimpse into the metabolic state of γ-secretase substrates, such as AβPP, in a specific brain region. Although physiological functions of p3-Alcα in brain and blood remain unclear, it is interesting to know the function for understanding the means of changes of p3-Alcα levels in aging and loss of cognitive functions. Analysis of more

cohorts should be performed to evaluate the changes of plasma p3-Alcα35 in subjects as an indicator of brain cognitive impairment such as that involved in AD.

ACKNOWLEDGMENTS

This work was supported in part by Grant-in-Aid for Scientific Research (SH and TS) from Ministry of Education, Culture, Sports, Science and Technology (MEXT), and a grant from the New Energy and Industrial Technology Development Organization (NEDO) in Japan. SH was supported by Astellas Foundation for Research on Metabolic Disorders and The Cell Science Research Foundation. We thank Drs. Yasuo Ihara and Ryozo Kuwano in J-ADNI for their critical discussion.

Authors' disclosures available online (http://www.j-alz.com/disclosures/view.php?id=1998).

SUPPLEMENTARY MATERIAL

Supplementary tables are available in the electronic version of this article: http://dx.doi.org/10.3233/JAD-131610.

REFERENCES

[1] Hintsch G, Zurlinden A, Meskenaite V, Steuble M, Fink-Widmer K, Kinter J, Sonderegger P (2002) The calsyntenins a family of postsynaptic membrane proteins with distinct neuronal expression patterns. *Mol Cell Neurosci* **21**, 393-409.

[2] Araki Y, Tomita S, Yamaguchi H, Miyagi N, Sumioka A, Kirino Y, Suzuki T (2003) Novel cadherin-related membrane proteins, Alcadeins, enhance the X11-like protein mediated stabilization of amyloid β-protein precursor metabolism. *J Biol Chem* **278**, 49448-49458.

[3] Kamal A, Stokin GB, Yang Z, Xia C-H, Goldstein LB (2000) Axonal transport of amyloid precursor protein is mediated by direct binding to the kinesin light chain subunit of kinesin-1. *Neuron* **28**, 449-459.

[4] Konecna A, Frischknecht R, Kinter J, Ludwig A, Steuble M, Meskenaite V, Indermuhle M, Engel M, Cen C, Mateos JM, Streit P, Sonderegger P (2006) Calsyntenin-1 docks vesicular cargo to kinesin-1. *Mol Biol Cell* **17**, 3651-3663.

[5] Araki Y, Kawano T, Taru H, Saito Y, Wada S, Miyamoto K, Kobayashi H, Ishikawa OH, Ohsugi Y, Yamamoto T, Matsuno K, Kinjyo M, Suzuki T (2007) The novel cargo receptor Alcadein induces vesicle association of kinesin-1 motor components and activates axonal transport. *EMBO J* **26**, 1475-1486.

[6] Kawano T, Araseki M, Araki Y, Kinjo M, Yamamoto T, Suzuki T (2012) A small peptide sequence is sufficient for initiating kinesin-1 activation through part of TPR region of KLC1. *Traffic* **13**, 834-848.

[7] Hata S, Fujishige S, Araki Y, Kato N, Araseki M, Nishimura M, Hartmann D, Saftig P, Fahrenholz F, Taniguchi M, Urakami K, Akatsu H, Martins RN, Yamamoto K, Maeda M, Yamamoto T, Nakaya T, Gandy S, Suzuki T (2009) Alcadein cleavages by APP α- and γ-secretases generate small peptides p3-Alcs indicating Alzheimer disease-related γ-secretase dysfunction. *J Biol Chem* **284**, 36024-36033.

[8] Piao Y, Kimura A, Urano S, Saito Y, Taru H, Yamamoto T, Hata S, Suzuki T (2013) Mechanism of intramembrane cleavage of Alcadeins by γ-secretase. *PLoS One* **8**, e62431.

[9] Araki Y, Miyagi N, Kato N, Yoshida T, Wada S, Nishimura M, Komano H, Yamamoto T, De Strooper B, Yamamoto K, Suzuki T (2004) Coordinated metabolism of Alcadein and amyloid β-protein precursor regulates FE65-dependent gene transactivation. *J Biol Chem* **279**, 24343-24354.

[10] Suzuki T, Nakaya T (2008) Regulation of amyloid β-protein precursor by phosphorylation and protein interactions. *J Biol Chem* **283**, 29633-29637.

[11] Rhinn H, Fujita R, Qiang L, Cheng R, Lee JH, Abeliovich A (2013) Integrative genomics identifies APOEε4 effectors in Alzheimer's disease. *Nature* **500**, 45-50.

[12] He X, Cooley K, Chung CH, Dashti N, Tang J (2007) Apolipoprotein receptor 2 and X11α/β mediate apolipoprotein E-induced endocytosis of amyloid-β precursor protein and β-secretase, leading to amyloid-β production. *J Neurosci* **27**, 4052-4060.

[13] Saito Y, Sano Y, Vassar R, Gandy S, Nakaya T, Yamamoto T, Suzuki T (2008) X11 proteins regulate the translocation of amyloid β-protein precursor (APP) into detergent-resistant membrane and suppress the amyloidogenic cleavage of APP by β-site-cleaving enzyme in brain. *J Biol Chem* **283**, 35763-35771.

[14] Saito Y, Akiyama M, Araki Y, Sumioka A, Shiono M, Taru H, Nakaya Y, Yamamoto T, Suzuki T (2011) Intracellular trafficking of the amyloid β-protein precursor (APP) regulated by novel function of X11-like. *PLoS One* **6**, e22108.

[15] Thinakaran G, Koo EH (2008) Amyloid precursor protein trafficking, processing, and function. *J Biol Chem* **283**, 29615-29619.

[16] Hata S, Fujishige S, Araki Y, Taniguchi M, Urakami K, Peskind E, Akatsu H, Araseki M, Yamamoto K, Martins N R, Maeda M, Nishimura M, Levey A, Chung KA, Montine T, Leverenz J, Fagan A, Goate A, Bateman R, Holtzman DM, Yamamoto T, Nakaya T, Gandy S, Suzuki T (2011) Alternative γ-secretase processing of γ-secretase substrates in common forms of mild cognitive impairment and Alzheimer disease: Evidence for γ-secretase dysfunction. *Ann Neurol* **69**, 1026-1031.

[17] Yanagida K, Okochi M, Tagami S, Nakayama T, Kodama TS, Nishitomi K, Jiang J, Mori K, Tatsumi S, Arai T, Ikeuchi T, Kasuga K, Tokuda T, Kondo M, Ikeda M, Deguchi K, Kazui H, Tanaka T, Morihara T, Hashimoto R, Kudo T, Steiner H, Haass C, Tsuchiya K, Akiyama H, Kuwano R, Takeda M (2009) The 28-amino acid form of an APLP1-derived Abeta-like peptide is a surrogate marker for Abeta42 production in the central nervous system. *EMBO Mol Med* **1**, 223-235.

[18] Mawuenyega KG, Sigurdson W, Ovod V, Munsell L, Kasten T, Morris JC, Yarasheski KE, Bateman RJ (2010) Decreased clearance of CNS β-amyloid in Alzheimer's disease. *Science* **330**, 1774.

[19] Kakuda N, Shoji M, Arai H, Furukawa K, Ikeuchi T, Akazawa K, Takami M, Hatsuta H, Murayama S, Hashimoto Y, Miyajima M, Arai H, Nagashima Y, Yamaguchi H, Kuwano R, Nagaike K, Ihara Y, Japanese Alzheimer's Disease Neuroimaging Initiative (2012) Altered γ-secretase activity in mild cognitive impairment and Alzheimer's disease. *EMBO Mol Med* **4**, 344-352.

[20] Benilova I, Karran E, De Strooper B (2012) The toxic Aβ oligomer and Alzheimer's disease: An emperor in need of clothes. *Nat Neurosci* **15**, 349-357.

[21] Konnno T, Hata S, Hamada Y, Horikoshi Y, Nakaya T, Saito Y, Yamamoto T, Yamamoto T, Maeda M, Gandy S, Akatsu H, Suzuki T, Japanese Alzheimer's Disease Neuroimaging Initiative (2011) Coordinate increase of γ-secretase reaction products in the plasma of some female Japanese sporadic Alzheimer's disease patients: Quantitative analysis with a new ELISA system. *Mol Neurodegener* **6**, 76.

[22] Hata S, Taniguchi M, Piao Y, Ikeuchi T, Fagan AM, Holzman DM, Bateman R, Sohrabi HR, Martins RN, Gandy S, Urakami K, Suzuki T, Japanese Alzheimer's Disease Neuroimaging, Initiative (2012) Multiple γ-secretase product peptides are coordinately increased in concentration in the CSF of a subpopulation of sporadic Alzheimer's disease subjects. *Mol Neurodegener* **7**, 16.

[23] Kamogawa K, Kohara K, Tabara Y, Takita R, Miki T, Konno T, Hata S, Suzuki T (2012) Utility of plasma levels of soluble p3-Alcadeinα as a biomarker for sporadic Alzheimer's disease. *J Alzheimers Dis* **31**, 421-428.

[24] Stephan BC, Brayne C, McKeith IG, Bond J, Mattews FE (2008) Mild cognitive impairment in the older population: Who is missed and does it matter? *Int J Geriart Psychiatry* **23**, 863-871.

[25] (1998) Cognitive function and dementia in six areas of England and Wales: The distribution of MMSE and prevalence of GMS organicity level in the MRC CFA Study. The Medical Research Council Cognitive Function and Ageing Study (MRC CFAS). *Psychol Med* **28**, 319-335.

[26] Morris JC (1993) The clinical dementia rating (CDR): Current version and scoring rules. *Neurology* **43**, 2412-2414.

[27] Lu J-X, Qiang W, Yau W-M, Schwieters CD, Meredith SC, Tycko R (2013) Molecular structure of β-amyloid fibriles in Alzheimer's disease brain tissue. *Cell* **154**, 1257-1268.

[28] Rohan de Silva HA, Jen A, Wickenden C, Jen LS, Wilkinson SL, Patel AJ (1997) Cell-specific expression of β-amyloid precursor protein isoform mRNAs and proteins in neurons and astrocytes. *Mol Brain Res* **47**, 147-156.

[29] Monning U, Konig G, Banati RB, Mechler H, Czech C, Gehrmann J, Schreiter-Gasser U, Masters CL, Beyreuther K (1992) Alzheimer βA4-amyloid protein precursor in immunocompetent cells. *J Biol Chem* **267**, 23950-23956.

Published in final edited form as:
Neuropathology. 2014 February ; 34(1): 11–18. doi:10.1111/neup.12055.

Immunohistochemical analysis of ubiquilin-1 in the human hippocampus: Association with neurofibrillary tangle pathology

Katsuyoshi Mizukami[1], **Eric E. Abrahamson**[2,4], **Zhiping Mi**[2], **Masanori Ishikawa**[5], **Kazushi Watanabe**[6], **Setsuo Kinoshita**[6], **Takashi Asada**[5], and **Milos D. Ikonomovic**[2,3,4]

[1]Graduate School of Comprehensive Human Sciences, University of Tsukuba, 3-29-1 Otsuka, Bunkyo-ku, Tokyo 112-0012, Japan

[2]Department of Neurology, University of Pittsburgh, Pittsburgh, PA 15213, USA

[3]Department of Psychiatry, University of Pittsburgh, Pittsburgh, PA 15213, USA

[4]Geriatric Research Education and Clinical Center, V.A. Pittsburgh Healthcare System, Pittsburgh, PA 15213, USA

[5]Department of Psychiatry, Institute of Clinical Medicine, University of Tsukuba, 1-1-1 Tennodai, Tsukuba city, Ibaraki 305-8575, Japan

[6]Proubase Technology Inc. 1-525-1-102 Kosugi-machi, Nakahara-ku, Kawasaki-city, Kanagawa 211-0063, Japan

Abstract

This postmortem immunohistochemical study examined the localization and distribution of ubiquilin-1 (UBL), a shuttle protein which interacts with ubiquitin and the proteasome, in the hippocampus from Alzheimer's disease (AD) dementia cases, and age-matched cases without dementia. Cases were stratified neuropathologically based on Braak staging for neurofibrillary tangles (NFT); cases without dementia were Braak stages 0-I-II (n=5), and AD cases were either Braak stages III–IV (n=7) or V–VI (n=11). In Braak stage 0-I-II cases, UBL immunoreactivity was detected in a dense fiber network in the neuropil, and in the cell cytoplasm and nucleoplasm of pyramidal neurons in CA fields and dentate gyrus granular neurons. In Braak stages III–IV and V–VI cases, UBL immunoreactivity was reduced in the neuropil and in the cytoplasm of the majority of CA1 neurons. In contrast, some CA1 pyramidal neurons and the majority of CA2/3 pyramidal, CA4 multipolar, and dentate granular neurons in Braak III–IV and Braak V–VI cases had markedly increased UBL immunoreactivity in the nucleoplasm. Dual immunofluorescence analysis of UBL and antibody clone AT8 revealed co-localization most frequently in CA1 pyramidal neurons in the Braak stage III–IV and V–VI cases. Further processing using the pan-amyloid marker X-34 revealed prominent UBL/X-34 dual labeling of extracellular NFT confined to the CA1/subiculum in the Braak stage V–VI cases. Our results demonstrate that in AD hippocampus, early NFT changes are associated with neuronal up-regulation of UBL in nucleoplasm, or its translocation from the cytoplasm to the nucleus. The perseverance of UBL

*Address correspondence and reprint requests to: Katsuyoshi Mizukami, MD, PhD, Graduate School of Comprehensive Human Sciences, University of Tsukuba, 3-29-1 Otsuka, Bunkyo-ku, Tokyo 112-0012, Japan, Tel: +81-298-53-3210 fax: +81-298-53-3183 kmizukami@taiiku.tsukuba.ac.jp

changes in CA2/3. CA4, and DG, generally considered as more resistant to NFT pathology, but not in the CA1, may mark a compensatory, potentially protective response to increased tau phosphorylation in hippocampal neurons; the failure of such a response may contribute to neuronal degeneration in end-stage AD.

Keywords

Alzheimer; amyloid; Plic-1; ubiquilin; tau

Introduction

The ubiquitin (Ub)–proteasome system is the major non-lysosomal proteolytic pathway in eukaryotes.[1] Ubiquilin-1 (also referred to as "protein linking integrin-associated protein to cytoskeleton 1", or Plic-1) is a Ub-like (UBL) protein with functional domains on its N-terminus (UB) and C-terminus (Ub-associated; UBA). Ubiquilin interacts with polyubiquitylated proteins through its UBA domain and with two subunits of the 19S proteasome through the UB domain.[2] UBL protein is observed in neurofibrillary tangles (NFT) in Alzheimer's disease (AD) brains[3], facilitates presenilin synthesis[3], and modulates amyloid precursor protein trafficking and amyloid-beta (Aβ) secretion.[4] Previous studies reported that early in AD, UBL-1 protein levels decrease in the frontal cortex[5]; the status of UBL-1 protein levels in the hippocampus in patients with varying degrees of NFT pathology is unknown. In this study, we used immunohistochemical techniques to examine localization and alterations in UBL-1 protein in the hippocampus from cases at different stages of NFT pathology as classified by Braak and Braak (1991)[6]. Multiple-label immunofluorescent microscopy analyses examined the relationship of UBL with early and late NFT changes. We hypothesized that changes in UBL-1 immunoreactivity intensity and/or cell type distribution are associated with the development and progression of NFT in AD hippocampus.

Methods

Hippocampal tissue was obtained postmortem from 23 cases: 18 with a clinical diagnosis of probable AD and five age-matched cognitively intact cases without AD pathology or with NFT confined to the entorhinal cortex. Clinical diagnosis of AD was based on a standardized ADRC evaluation at a Consensus Conference, utilizing DSM-IV[7] and NINCDS/ADRDA[8] criteria. Demographic and neuropathology data are presented in Table 1. Neuropathological diagnosis was determined by a certified neuropathologist using CERAD[9] and NIA-Reagan Consensus criteria[10] (Table 1). All cases in the study were classified into stages 0 to VI according to Braak and Braak[6] (Table 1). One case (Braak stage IV) had a family history of AD.

Brain tissue was processed according to previously described procedures.[11,12] Blocks from the middle of the hippocampal body were cut in a coronal plane and placed in 0.1 M sodium phosphate buffer (PB, pH = 7.4) containing 4% paraformaldehyde for 48 h at 4°C and then cryoprotected by immersion in 30% sucrose in PB for no longer than seven days. The tissue was then frozen, sectioned at 40 μm, and processed for immunohistochemistry as previously

described.[11,12] Sections were immunolabeled using a rabbit polyclonal antibody against ubiquilin 1 (U7258, Sigma, Lot# E0409, 1:1000), generated against an immunogen corresponding to carboxy terminus amino acids 502–519 of human ubiquilin-1. This antibody recognizes human ubiquilin-1 as a 62 kDa band on Western blot; this band is eliminated when the antibody is pre-incubated with the immunizing peptide (Sigma, manufacturer details). Furthermore, the immunoreactivity pattern observed using this antibody closely mirrors the pattern observed in a previous investigation of UBL-1 expression in AD brain[3], both in the pattern of subcellular localization (cytoplasm and nucleoplasm; see below) and association with NFT (see below). Multiple labeling immunofluorescence was performed as described previously[13]. Sections were incubated overnight in a primary antibody cocktail consisting of rabbit anti-UBL (1:1,000; antibody specifics described above) and mouse monoclonal antibody clone AT8 (1:2,000; epitope on tau phosphorylated at Ser202[14], Thermo Scientific, catalogue #MN1020, Lot #KK138691) in 1% normal goat serum for 24 hours at 4°C. Indirect immunofluorescence was achieved using a cocktail of goat anti-rabbit antisera conjugated to Alexa 488 (Molecular Probes, catalogue #A-11034, Lot #93C1-1) and goat anti-mouse antisera conjugated to Alexa 594 (Molecular Probes, catalogue #A-11032, Lot #93C1-1), both diluted 1:250 in 1% normal goat serum. Processed sections were mounted onto gelatin-coated slides and coverslipped with Fluoromount (SouthernBiotech). Immunofluorescent signal was detected using an Olympus BX53 upright microscope, the X-Cite 120Q excitation light source (Lumen Dynamics), an Olympus DP72 digital camera, and CellSens Standard 1.6 image acquisition software (Olympus). After initial analysis of UBL and AT8 immunofluorescence, slides were decoverslipped by immersion in PB, counterstained with the pan-amyloid binding dye, X-34, a highly fluorescent derivative of Congo red which detects NFT and Aβ plaques with greater sensitivity than thioflavin-S,[15,16] and coverslipped with Vectashield Hard Set mounting medium with a DNA-specific fluorescent probe DAPI (Vector). Sections were then reanalyzed; X-34 did not interfere with either immunofluorescent marker signal, and was distinguished easily from the DAPI labeling of cell nuclei. Confirmation of fluorescence co-labeling of the four fluorescent markers was achieved using an Olympus BX51 upright microscope equipped with an Olympus DSU spinning disk confocal and motorized stage controlled by both StereoInvestigator (Version 8.0, MBF Bioscience) and SlideBook 4.2 (Intelligent Imaging Innovations) software, using Lumen200Pro metal halide illumination and a 60X 1.4 N.A. oil immersion objective. The four fluorescent markers were completely dissociable by color (UBL, AT8, X-34/DAPI) and subcellular localization (X-34, DAPI). Additional sections from each case were processed with cresyl violet to delineate the cytoarchitectural boundaries of the hippocampus as defined by Duvernoy[17]. Two independent evaluators determined intensity of the chromogen-based UBL immunoreactivity qualitatively on a scale from 0 (no immunoreactivity) to ++++ (most intense immunoreactivity, see Table 2). To reflect the variability in the immunoreactive signal between neurons in CA1 region of the Braak stage III–IV group, two scores are presented (Table 2). Quantification of chromogen-based UBL immunohistochemical optical density was performed as described previously[18] using Image J freeware. [19] Optical density was measured in the cytoplasm and nucleoplasm of pyramidal neurons in the CA1 and CA2/3 fields, and multipolar neurons in the CA4 field. Due to individual variation in overall intensity of UBL-ir between cases in each Braak staged group, analyses are presented as the

ratio of nucleoplasm-to-cytoplasm optical density values in the same sections/cases. Data was compared using the Kruskal Wallis test with Dunn's multiple comparison post hoc test, and Spearman rank order correlation tests, as the data did not conform to the prerequisites for parametric statistical testing. Significance values less than $p = 0.01$ (non-directional) were considered statistically significant.

Results

There were no statistically significant differences in demographics between the three Braak stage groups although the Braak stage 0-I-II (non-AD) group trended towards younger age ($p = 0.013$ by Kruskal-Wallis, no differences were detected with Dunn's multiple comparison test). UBL immunoreactivity had distinct patterns in the three Braak stage groups (described below), and localization was almost exclusively neuronal in all groups, with only in 2/11 cases (one Braak stage VI, one Braak stage IV with family history of AD) exhibiting UBL immunoreactivity in cells with the morphological appearance of microglia and oligodendrocytes, and located throughout the gray and white matter, respectively (not shown). In Braak stage 0-I-II cases (NFT absent or confined to the entorhinal cortex), UBL immunoreactivity was observed in the neuropil in the stratum pyramidale of the Ammon's horn (CA) and molecular layer of the dentate gyrus (DG). UBL immunoreactivity was also detected in neuronal soma, dendrites, and in the nucleoplasm in hippocampal neurons, including pyramidal and multipolar neurons in the CA fields, and DG granular neurons. In the majority of neurons, UBL immunoreactivity intensity was higher in the nucleoplasm compared to the cytoplasm (Figure 1; Table 2). UBL immunoreactivity in the nucleoplasm appeared punctuate/vesicular (Figure 1 inset a; Figure 4A) and was most prominent in the CA2/3 field (Table 2).

In Braak stage III–IV cases (NFT involving the entorhinal cortex and hippocampus but not neocortex), UBL immunoreactivity in the neuropil was reduced in the CA1 and CA2/3 regions, and was unchanged in the CA4 and DG, compared to Braak stage 0-I-II cases. The majority of CA1 neurons exhibited reduced cytoplasmic and nucleoplasmic labeling, however a subset of CA1 pyramidal neurons had prominent UBL immunoreactivity in the nucleoplasm (Figure 1B). The intensity of UBL immunoreactivity in the nucleoplasm increased markedly in the majority of CA2/3 pyramidal neurons, CA4 multipolar neurons, and DG granular neurons (Figure 1E; 2 H,K; Table 2). We also observed UBL immunoreactivity in fibers in the CA2/3 radiatum/moleculare and DG molecular layer in three of the Braak stage III–IV cases (Braak III: 1; Braak IV: 2; not shown).

In Braak stage V–VI cases, UBL immunoreactivity was less intense in the CA1 field, both in the neuropil and in pyramidal neurons, except those with the morphological appearance of extracellular NFT (eNFT), where UBL immunoreactivity was prominent (Figure 1C. inset c). In contrast, UBL immunoreactivity in neuropil and neuronal cytoplasm in CA2/3, CA4, and dentate gyrus was similar to the pattern observed in Braak stage III–IV cases, albeit with a less prominent increase in nucleoplasmic UBL immunoreactivity (Figure 1F,I,L; Table 2).

Analysis of UBL immunoreactivity optical density confirmed a significant increase ($p < 0.0001$) in the nucleoplasm/cytoplasm optical density ratio in the CA1 field from Braak

stages 0-I-II compared to Braak stages III–IV (Figure 2; in Braak stages V–VI, small numbers of UBL immunoreactive pyramidal cells remaining in the CA1 precluded optical density analyses). The ratio was slightly, but non-significantly, elevated in the CA2/3 field from Braak stage groups III–IV and V–VI when compared to Braak stage group 0-I-II, and a similar trend was observed in the CA4 field (Figure 2). Optical density measurements in the nucleoplasm and cytoplasm correlated directly across all Braak staged groups in CA2/3 as well as in CA4, but did not correlate in the CA1 field (data not shown). We detected statistically significant (Spearman $r = 0.7$, $p = 0.01$) correlation between more advanced age and higher nucleoplasm/cytoplasm UBL immunoreactivity optical density ratio values in CA1, but not CA2/3 or CA4.

The relationship between UBL protein and a marker of advanced stage NFT including extracellular "ghost NFT" (X-34) or an antibody that also recognizes pre/early NFT (AT8) was examined using multiple-label fluorescence confocal microscopy (Figures 3, 4). The pattern of UBL immunofluorescence was consistent with our observations using the same antibody and chromogen-based immunohistochemistry with light microscopy (Figure 3). In multiple-labeled (UBL, AT8, DAPI, X-34) sections from Braak stage 0-I-II cases, we observed pyramidal neurons with UBL-immunofluorescence in the cytoplasm and nucleoplasm, the latter co-labeled with DAPI (Figure 3A–D). Braak 0-I-II cases had no AT8 or X-34 postitive NFT in the hippocampus, though sparse, scattered AT8 immunofluorescent neuritic elements were observed in the CA fields (Figure 3E–H). In Braak staged III–IV and V–VI cases, we observed a complex pattern of UBL/AT8 or UBL/X-34 co-localization in CA fields. Neurons with light cytoplasmic and prominent nucleoplasmic UBL immunofluorescence co-localized AT8, but had little or no X-34, (Figure 3I–L, M–P, M′–P′). The majority of UBL-immunofluorescent pyramidal neurons in the CA2/3 region were AT8- and X34-negative, yet surrounded by numerous AT8-immunofluorescent neurites (Figure 3I–L). Pyramidal neurons in CA1 and subiculum of Braak staged V–VI cases had UBL immunofluorescence co-localized with X-34, and very little or no AT8 immunofluorescence and no DAPI labeling, indicative of extracellular 'ghost' NFT (eNFT, Figure 3M–P, M″–P″). UBL immunoreactive neuritic elements were also detected within X-34 labeled amyloid plaques in the CA1 and DG molecular layer (not shown). A small number of AT8 positive neurons lacking UBL immunofluorescence were observed in the CA1 region of Braak V–VI cases. The overall pattern of UBL/AT8/X-34 immunofluorescence in a representative Braak stage VI case is illustrated diagrammatically in Figure 4.

Discussion and Conclusion

The present study investigated UBL immunoreactivity in the hippocampus from non-AD and clinically-diagnosed AD cases stratified by Braak stages, in relation to markers of primarily advanced stage NFT (the pan-amyloid marker X-34) and the antibody clone AT8 which also recognizes pre/early NFT. We report two novel findings: 1) with the emergence of NFT in the hippocampus, UBL immunoreactivity in pyramidal neurons changes from cytoplasmic/nuclear to predominantly nuclear localization and, in a subset of neurons, co-localizes with phosphorylated tau and 2) prominent UBL immunoreactivity is present in a subset of end-stage, extracellular NFT (eNFT) in the CA1/subiculum. Neurons in CA2-4

fields and DG, generally spared from classic NFT pathology development in AD, exhibited markedly increased UBL immunoreactivity in the nucleoplasm in Braak stages III–IV and V–VI AD cases compared to the Braak 0-I-II group. The reason for this change is unknown, but it may be influenced by age differences between Braak groups, since the Braak stage 0-I-II (non-AD) group trended towards being younger than both the Braak stage III–IV and Braak stage V–VI AD groups. Other factors, including nucleotide polymorphisms in the ubiquilin gene, may contribute to the observed differences and warrant future clinical-genetic-pathological studies. Genetic abnormalities in UBL-1 were reported to associate with increased risk[20] and age of onset and duration[21] of AD, although this association was not replicated in all studies.[22] Because Braak staged groups represent a continuum, rather than a stepwise progression, of NFT pathology, the large variability in UBL intensity ratios in the Braak stage III–IV group, particularly in the CA1 region, is likely due to variability in the extent of pathologic changes, and UBL expression, in individual pyramidal neurons.

The functional relevance of the changes in the subcellular localization of UBL, and their association with different types of NFT, is unknown but it may reflect a response, compensatory or dysregulatory, of the ubiquitin-proteosome system to increased cellular stress due to accumulation of aggregated and heavily-phosphorylated proteins, especially tau. Our observation of increased UBL immunoreactivity in X-34 positive eNFT is particularly intriguing considering that ubiquitin, a major component of NFT's paired helical filaments in AD, [23,24] is largely absent from eNFT. [23, 25, 26] These changes may occur in relation to ubiquitin-proteosome dysfunction or, alternatively, they may reflect altered antigenic profiles of these proteins in eNFT.[27] The observation of UBL immunoreactivity in X-34 positive neuritic plaques in advanced Braak stages further suggests a relationship between UBL and tau changes, and warrants further exploration. Furthermore, the source of the fibers that comprise UBL immunoreactive dystrophic neurites, and the significance of these changes in the pathogenesis of neuritic plaques, is unknown. Further investigation is also warranted regarding the observation of UBL immunoreactive cells with the morphological appearance of microglia and oligodendrocytes in the hippocampus of two AD cases, especially when considering that one case had a family history of AD. Ubiquilin is up-regulated in glial cells in some pathologic conditions including hypoxia,[28] thus glial cells could increase ubiquilin 1 expression due to cell stress induced by neurofibrillary pathology. Alternatively, these observations may be indicative of differences in subjects' agonal state.

In conclusion, these results demonstrate that in AD hippocampus, UBL immunoreactivity increases in the neuronal nucleoplasm and is associated with region-specific neurofibrillary changes. Up-regulation of UBL could contribute to pathology progression, or reflect a compensatory response. Future studies examining the link between UBL and NFT as well as other types of AD pathology are warranted.

Acknowledgments

We are indebted to the support of the participants in the ADRC at the University of Pittsburgh. This study was supported by NIH grants NIA AG05133 (University of Pittsburgh ADRC), AG014449 and AG025204 (MDI), The Snee-Reinhardt Charitable Foundation (MDI), and by a Grant-in-Aid for Scientific Research from the Japanese Ministry of Education, Culture, Sports, Science and Technology (KM). Ms. Suganya Srinivasan, Ms. Lan Shao, Ms. Natsuko Kato and Ms. Megumi Mitani provided expert technical assistance.

References

1. Hershko A, Ciechanover A. The ubiquitin system. Annu Rev Biochem. 1998; 67:425–479. [PubMed: 9759494]
2. Ko HS, Uehara T, Tsuruma K, Nomura Y. Ubiquilin interacts with ubiquitylated proteins and proteasome through its ubiquitin-associated and ubiquitin-like domains. FEBS Letters. 2004; 566:110–114. [PubMed: 15147878]
3. Mah AL, Perry G, Smith MA, Monteiro MJ. Identification of ubiquilin, a novel presenilin interactor that increases presenilin protein accumulation. J Cell Biol. 2000; 151:847–862. [PubMed: 11076969]
4. Hiltunen M, Lu A, Thomas AV, et al. Ubiquilin 1 modulates amyloid precursor protein trafficking and Aβ secretion. J Biol Chem. 2006; 281:32240–32253. [PubMed: 16945923]
5. Stieren ES, El Ayadi A, Xiao Y, et al. Ubiquilin-1 is a molecular chaperone for the amyloid precursor protein. J Biol Chem. 2011; 286:35689–35698. [PubMed: 21852239]
6. Braak H, Braak E. Neuropathological staging of Alzheimer-related changes. Acta Neuropathol (Berl). 1991; 82:239–259. [PubMed: 1759558]
7. American Psychiatric Association. Diagnostic and statistical manual of mental disorders. 4. Washington, D.C: American Psychietric Association; 1994.
8. McKhann G, Drachman D, Folstein M, Katzman R, Price D, Stadlan EM. Clinical diagnosis of Alzheimer's disease: Report of Health and Human Services Task Force on Alzheimer's disease. Neurology. 1984; 34:939–944. [PubMed: 6610841]
9. Mirra SS, Heyman A, McKeel D, et al. The consortium to establish a registry for Alzheimer's disease (CERAD). Part II. Standardization of the neuropathologic assessment of Alzheimer's disease. Neurology. 1991; 41:479–486. [PubMed: 2011243]
10. Consensus report of the Working Group on "Molecular and Biochemical Markers of Alzheimer's Disease". The Ronald and Nancy Reagan Research Institute of the Alzheimer's Association and the National Institute on Aging Working Group. Neurobiol Aging. 1998; 19:109–116. [PubMed: 9558143]
11. Mizukami K, Ikonomovic MD, Grayson DR, et al. Immunohistochemical study of GABAA receptor β2/3 subunits in the hippocampal formation of aged brains with Alzheimer-related neuropathologic changes. Exp Neurol. 1997; 147:333–345. [PubMed: 9344558]
12. Iwakiri M, Mizukami K, Ikonomovic MD, et al. An immunohistochemical study of GABA receptor gamma subunits in Alzheimers disease hippocampus: relationship to neurofibrillary tangle progression. Neuropathology. 2009; 29:263–269. [PubMed: 19019179]
13. Ikonomovic MD, Abrahamson EE, Uz T, Manev H, Dekosky ST. Increased 5-lipoxygenase immunoreactivity in the hippocampus of patients with Alzheimer's disease. J Histochem Cytochem. 2008; 56:1065–1073. [PubMed: 18678882]
14. Mercken M, Vandermeeren M, Lübke U, et al. Monoclonal antibodies with selective specificity for Alzheimer Tau are directed against phosphatase-sensitive epitopes. Acta Neuropathol. 1992; 84:265–272. [PubMed: 1384266]
15. Styren SD, Hamilton RL, Styren GC, Klunk WE. X-34, a fluorescent derivative of Congo red: a novel histochemical stain for Alzheimer's disease pathology. J Histochem Cytochem. 2000; 48:1223–1232. [PubMed: 10950879]
16. Ikonomovic MD, Abrahamson EE, Isanski BA, et al. X-34 labeling of abnormal protein aggregates during the progression of Alzheimer's disease. Methods Enzymol. 2006; 412:123–144. [PubMed: 17046656]
17. Duvernoy, HM. The Human Hippocampus. Munchen: JF Bergmann Verlag; 1988.
18. Iwakiri M, Mizukami K, Ikonomovic MD, et al. Changes in hippocampal GABABR1 subunit expression in Alzheimer's patients: association with Braak staging. Acta Neuropathol. 2005; 109:467–474. [PubMed: 15759131]
19. Rasband, WS. ImageJ. U. S. National Institutes of Health; Bethesda, Maryland, USA: 1997–2012. http://imagej.nih.gov/ij/
20. Bertram L, Hiltunen M, Parkinson M, et al. Family-based association between Alzheimer's disease and variants in UBQLN1. N Engl J Med. 2005; 352:884–894. [PubMed: 15745979]

21. Kamboh MI, Minster RL, Feingold E, DeKosky ST. Genetic association of ubiquilin with Alzheimer's disease and related quantitative measures. Mol Psychiatry. 2006; 11:273–279. [PubMed: 16302009]
22. Smemo S, Nowotny P, Hinrichs AL, et al. Ubiquilin 1 polymorphisms are not associated with late-onset Alzheimer's disease. Ann Neurol. 2006; 59:21–26. [PubMed: 16278862]
23. Mori H, Kondo J, Ihara Y. Ubiquitin is a component of paired helical filaments in Alzheimer's disease. Science. 1987; 235:1641–1644. [PubMed: 3029875]
24. Perry G, Friedman R, Shaw G, et al. Ubiquitin is detected in neurofibrillary tangles and senile plaque neurites of Alzheimer disease brains. Proc Natl Acad Sci U S A. 1987; 84:3033–3036. [PubMed: 3033674]
25. Ikeda K, Haga C, Oyanagi S, et al. Ultrastructural and immunohistochemical study of degenerate neurite-bearing ghost tangles. J Neurol. 1992; 239:191–194. [PubMed: 1597685]
26. Kobayashi K, Muramori F, Aoki T, et al. KP-1 is a marker for extraneuronal neurofibrillary tangles and senile plaques in Alzheimer diseased brains. Dement Geriatr Cogn Disord. 1998; 9:13–19. [PubMed: 9469259]
27. Bancher C, Brunner C, Lassmann H, et al. Tau and ubiquitin immunoreactivity at different stages of formation of Alzheimer neurofibrillary tangles. Prog Clin Biol Res. 1989; 317:837–848. [PubMed: 2557644]
28. Ko HS, Uehara T, Nomura T. Role of ubiquilin associated with protein-disulfide isomerase in the endoplasmic reticulum in stress-induced apoptotic cell death. J Biol Chem. 2002; 277:35386–35392. [PubMed: 12095988]

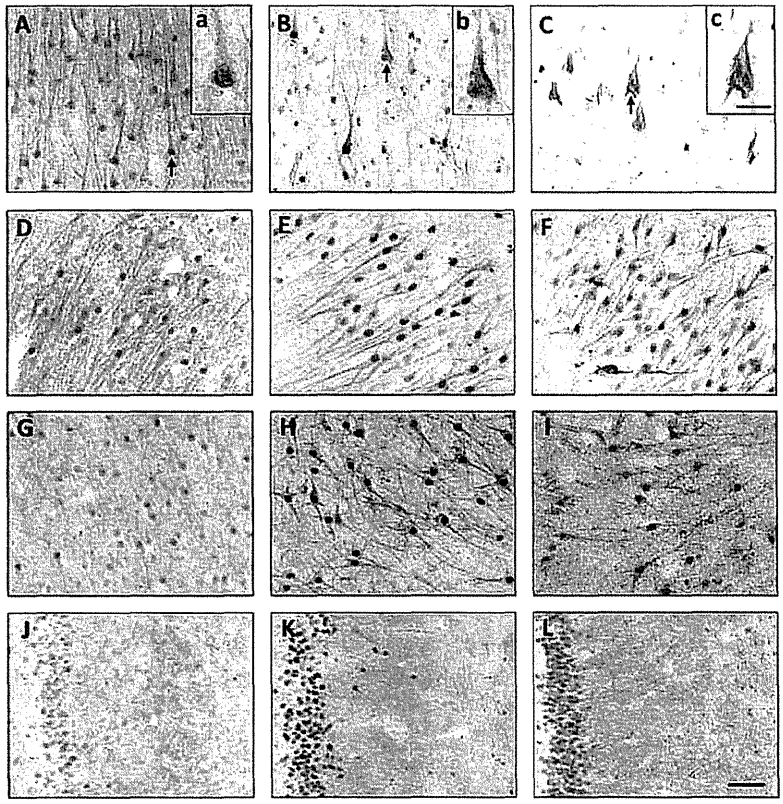

Fig. 1.

Photomicrographs showing ubiquilin (UBL) immunoreactivity in CA1 (A–C), CA2/3 (D–F), CA4 (G–I), and dentate gyrus (J–L; molecular layer is on the right) hippocampal fields in cases representative of Braak stages 0-I-II (A,D,G,J), Braak stages III–IV (B,E,H,K), and Braak stages V–VI (C,F,I,L) groups. In the CA1 field, representative UBL-ir pyramidal neurons (arrows) are illustrated at a higher magnification in the insets (a–c). Scale bar = 50 μm (A–L); 20 μm (a–c).

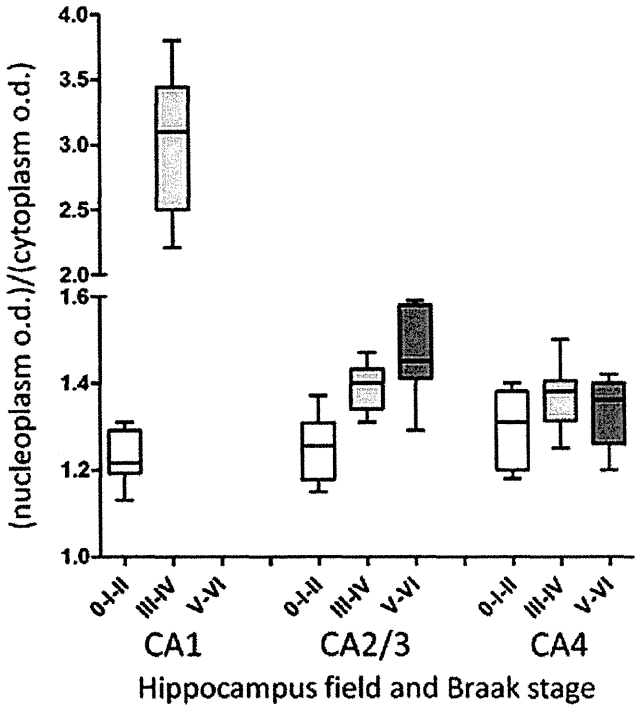

Fig. 2.

Box and whiskers graphs represent results from optical density measurements of ubiquilin-immunohistochemistry in the CA1, CA2/3, and CA4 hippocampus fields in cases with Braak stages 0-I-II, III–IV, and V–VI. Due to high variability in the intensity of UBL-immunoreactivity across cases, data were expressed as a ratio of the values obtained from the nucleoplasm and cytoplasm. There were insufficient pyramidal neurons in CA1 hippocampus in Braak group staged V–VI to perform the analysis. Box plots describe the following: whiskers, maximum and minimum values; line within box, median; upper and lower limits of box, upper and lower quartiles.

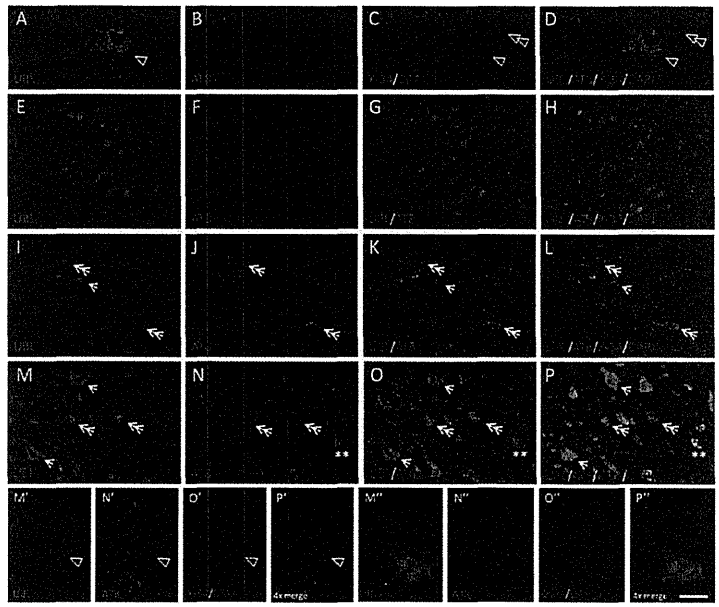

Fig. 3.

Multiple-label fluorescent microscopy analyses of associations between ubiquilin (UBL) and markers of NFT (antibody clone AT8 and amyloid dye X-34). A–D: Confocal imaging of UBL immunofluorescence (A, green) in the nucleoplasm and cytoplasm of a large pyramidal neuron in the CA1 region of the hippocampus from a Braak stage I case. The nucleoplasm is co-labeled with the DNA binding compound 4′,6-diamidino-2-phenylindole (C, D, single arrowhead; DAPI). The nucleus of an adjacent glial cell is also prominently DAPI-labeled but it lacks UBL immunoreactivity (C,D, double arrowhead). There are only small amounts of AT8 immunofluorescence and X-34 histofluorescence in some neuritic processes, but not in neuronal cell bodies (B,D). E–H: UBL immunofluorescence (E,G,H green) in the nucleoplasm and cytoplasm of neurons in the CA3 region of the hippocampus from a Braak stage II case. AT8-immunofluorescence is scarce, restricted to neurites scattered in the neuropil (F–H, red). UBL-immunofluorescent neurons exhibit prominent nuclear labeling with DAPI (H). No X-34 positive tangles are present (H). I–L: UBL immunofluorescence (I,K,L, green) in the nucleoplasm and cytoplasm of neurons in the CA3 region of the hippocampus from a Braak stage IV case. AT8-immunofluorescence is observed in neurites (J–L red) scattered in the neuropil and in the cytoplasm of some pyramidal neurons (J, double arrowheads); these neurons are co-labeled with UBL in the cytoplasm and nucleoplasm (K, double headed arrows). A UBL positive cell that lacks AT8 labeling is indicated by an arrow. UBL and UBL/AT8 immunofluorescent neurons are co-labeled with DAPI but do not contain X-34 histofluorescence (L). M–P: UBL immunofluorescence (M, O, P, green) in the CA1 region of the hippocampus from a Braak stage VI case, co-labeled with AT8 (O), DAPI and X-34 (P, all four markers merged). UBL and AT8 co-localize in the cytoplasm of a subset of neurons which contain UBL (and DAPI) positive nucleus but are devoid of X-34 signal (P; double arrows). UBL is detectable in a subset of X-34 positive extracellular NFT (NFT lacking detectable nucleus) that exhibit little, if any, AT8 signal (M,O,P; arrows). AT8 positive intracellular NFT with no detectable UBL immunofluorescence are also detected (N–P; double asterisk). M′–P′: Confocal microscopic image of UBL immunofluorescence in the cytoplasm and nucleoplasm (M′, green) of an AT8-positive intracellular NFT with DAPI-confirmed nucleus (O′–P′) in the CA1. M″–P″: Confocal microscopic image of UBL immunofluorescence (M″, green) in an extracellular NFT (devoid of DAPI signal) with prominent X-34 co-labeling (O″–P″) and very little AT8 signal (N″) in the CA1. Scale bar = 7 μm (A–D), 40 μm (E–H), 30 μm (I–P), 14 μm (M′–P″).

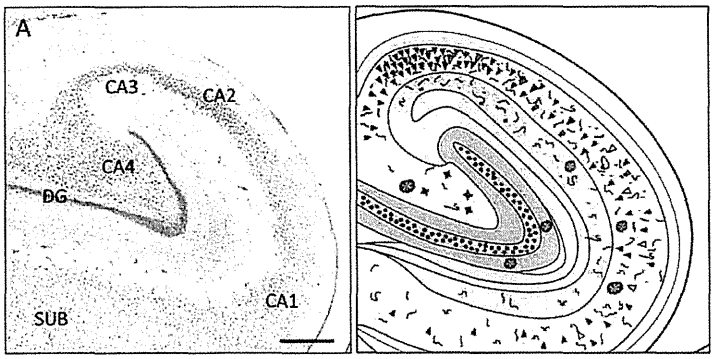

Fig. 4.

A. Sub-regional division of the hippocampus illustrated in a Nissl stained section. CA1, CA2, CA3, CA4 = Cornu Ammonis fields 1–4; DG = dentate gyrus, SUB = subiculum. Scale bar = 200 μm. B. Schematic illustration of the pattern of ubiquilin, AT8, and X-34 fluorescence in the hippocampus from a representative Braak stage VI case.

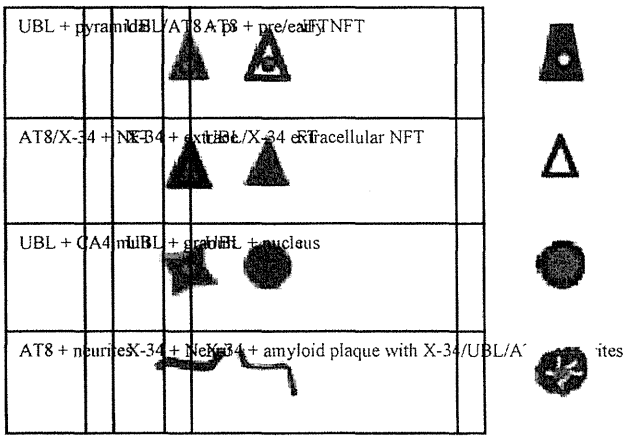

Table 1

Case demographic data.

Demographic	Braak stage 0-I-II	Braak stage III–IV	Braak stage V–VI
Number of cases			
(N)	3-1-1	3–4	4–7
[1]**Age (years)**			
Mean (SD)	61.4 (9)	78.5 (7.2)	75.2 (10.5)
Range	48–71	68–90	63–91
CERAD diagnosis	Not AD (5)	Probable (7)	Definite (11)
[2]**NIA-Reagan diagnosis**	Low (5)	Intermediate (7)	High (11)
Brain weight (g)			
Mean (SD)	1120 (346.3)	1192 (161.7)	1110 (137.9)
Range	690–1600	970–1350	930–1300
PMI (hours)			
Mean (SD)	5.8 (1.5)	6 (2.5)	6.5 (2.7)
Range	4–8	2–9	2–17
Sex			
(Male)	1-0-1	2–3	1–2
Aβ deposits			
(Present)	0-0-1	3–4	4–7
[3]**Co-neuropsychiatric**			
(Present)	0-0-1	0-0	2–4
[4]**Co-pathology**			
(Present)	3-0-0	1–2	0–1
Race			
(White)	2-1-1	2–4	4–7

[1] $p = 0.013$ (Kruskal-Wallis); $p < 0.01$ (Dunn's multiple comparison test).

[2] Likelyhood of Alzheimer's disease

[3] Braak stage 0-I-II: Frontotemporal dementia; Braak stage V–VI: abuse (V – indicates Braak stage), delusions (V, VI, VI), depression (V, VI) (all separate).

[4] Braak stage 0-I-II: Pick's disease (0), Corticobasal degeneration (0), MND-inclusion dementia (0) (all separate); Braak stage III–IV: DLB mild (III), DLB severe (IV, IV); Braak stage V–VI: DLB severe (VI).

Abbreviations: Aβ, amyloid-beta peptide; DLB, Lewy bodies; g, grams; MND, motor neuron disease; N, number of subjects; PMI, post mortem interval; SD, standard deviation.

Table 2

Qualitative analysis of ubiquilin-1 immunoreactivity intensity in the hippocampus from cases staged Braak 0-I-II, III–IV, and V–VI).

	NEUROPIL				NEURONAL CYTOPLASM				NEURONAL NUCLEOPLASM			
	CA1	CA2/3	CA4	DG	CA1	CA2/3	CA4	DG	CA1	CA2/3	CA4	DG
Braak 0-I-II	++	++	++	+	++	++	+	+	++	+++	++	+
Braak III–IV	+	+	++	+	0/+	++	++	++	+	++++	++++	++
Braak V–VI	+	+	++	+	+	+	+	++	+	+++	+++	++

Abstract Send to:

See 1 citation found by title matching your search:

Int J Soc Psychiatry. 2014 May;60(3):290-8. doi: 10.1177/0020764013486777. Epub 2013 Jun 5.

How perceived social support relates to suicidal ideation: a Japanese social resident survey.

Endo G[1], Tachikawa H, Fukuoka Y, Aiba M, Nemoto K, Shiratori Y, Matsui Y, Doi N, Asada T.

Author information

Abstract

BACKGROUND: The loss of social support is one of the major risk factors for suicide. However, there are few empirical studies that have examined how a person's suicide ideation relates to their social support.

AIMS: To examine the relationship between social support and suicidal ideation.

METHODS: Self-report questionnaires were sent to 2,200 randomly selected adults in Japan. The questionnaire inquired the participants about the severity of suicidal ideation, the details of current perceived social support and their degree of satisfaction with this social support. Social support and related indicators were compared among three groups of participants that varied in severity of suicidal ideation.

RESULTS: People in the group that had suicide ideation during their lives reported receiving significantly less support from their family and had greater feelings of dissatisfaction with that support than those in the other groups. Furthermore, people who had suicide ideation during the month immediately preceding the survey reported providing less support to their family, relatives or friends, as well as receiving less support from family than other groups, and having stronger feelings of dissatisfaction with social support.

CONCLUSION: Our study identified a strong relationship between the severity of suicidal ideation and perceived social support.

KEYWORDS: *Japan; Suicidal ideation; questionnaire; resident survey; social support*

PMID: 23741005 [PubMed - indexed for MEDLINE]

Abstract Send to:

See 1 citation found by title matching your search:

Psychiatry Clin Neurosci. 2014 Apr;68(4):299-307. doi: 10.1111/pcn.12132. Epub 2014 Jan 9.

Network analysis for motives in suicide cases: a cross-sectional study.

Shiratori Y[1], Tachikawa H, Nemoto K, Endo G, Aiba M, Matsui Y, Asada T.

Author information

Abstract

AIM: Suicide victims have various distresses or motives. There are few studies on how these motives toward suicide relate with each other. We used network analyses to extract the structures of correlations among the motives for suicide.

METHODS: We obtained datasets of suicide victims from 2007-2009 in Japan in cooperation with Ibaraki Prefectural Police Headquarters. The data were analyzed by network centrality measures and a structural analysis by block modeling.

RESULTS: Among the motives, depression and physical illness showed relatively high scores of 'degree centrality', whereas depression and unemployment showed relatively high scores of 'betweenness centrality'. Structural analysis by block modeling resulted in eight blocks. The most important block comprised eight motives, including conflict between parent and child, marital conflict, economic hardship, and overloaded with debt.

CONCLUSION: Depression and physical illness were important and priority areas for completed suicides, although these two motives had different influences on suicide behaviors. Furthermore, structural analysis revealed the important role of a block, including some familial and financial motives, which induced hopelessness. Our results suggest that it might be useful to consider the common ways in which motivations for suicide are tied together when suicide intervention is launched from a social model point of view.

KEYWORDS: completed suicide; hopelessness; motive; network analysis; police statistics

PMID: 24405435 [PubMed - indexed for MEDLINE]

Publication Types, MeSH Terms

LinkOut - more resources

PubMed Commons

PubMed Commons home

0 comments

How to join PubMed Commons

Save items

Add to Favorites

Related citations in PubMed

Differences in recent life events between alcoholic and depre: [Alcohol Clin Exp Res. 1994]

Are some motives more linked to suicide proneness than others? [J Clin Psychol. 1998]

Childhood bullying behaviors as a risk for suicide attempts an [J Am Acad Child Adolesc Psychi...]

Review Prevention of suicide and attempted suicide in Denmark. Epiden [Dan Med Bull. 2007]

Review Jobless. Unemployment and young people's health. [Med J Aust. 1998]

See reviews...

See all...

Related information

Related Citations

MedGen

Search details

```
Network[Title] AND
analysis[Title] AND
motives[Title] AND suicide[Title]
AND cases[Title] AND cross-
sectional[Title] AND study[Title]
```

Search See more...

Recent Activity

Turn Off Clear

Network analysis for motives in suicide cases: a cross-sectional study. PubMed

Network[Title] AND analysis[Title] AND motives[Title] AND suicide... (1) PubMed

How perceived social support relates to suicidal ideation: a Japanese social r PubMed

perceived[Title] AND social[Title] AND support[Title] AND relates... (1) PubMed

Increased levels of plasma p3-alcα35, a major fragment of Alcadeinα by γ-sec PubMed

Visual-Statistical Interpretation of ^{18}F-FDG-PET Images for Characteristic Alzheimer Patterns in a Multicenter Study: Inter-Rater Concordance and Relationship to Automated Quantitative Evaluation

T. Yamane, Y. Ikari, T. Nishio, K. Ishii, K. Ishii, T. Kato, K. Ito, D.H.S. Silverman, M. Senda, T. Asada, H. Arai, M. Sugishita, T. Iwatsubo, and the J-ADNI Study Group

ABSTRACT

BACKGROUND AND PURPOSE: The role of ^{18}F-FDG-PET in the diagnosis of Alzheimer disease is increasing and should be validated. The aim of this study was to assess the inter-rater variability in the interpretation of ^{18}F-FDG-PET images obtained in the Japanese Alzheimer's Disease Neuroimaging Initiative, a multicenter clinical research project.

MATERIALS AND METHODS: This study analyzed 274 ^{18}F-FDG-PET scans (67 mild Alzheimer disease, 100 mild cognitive impairment, and 107 normal cognitive) as baseline scans for the Japanese Alzheimer's Disease Neuroimaging Initiative, which were acquired with various types of PET or PET/CT scanners in 23 facilities. Three independent raters interpreted all PET images by using a combined visual-statistical method. The images were classified into 7 (FDG-7) patterns by the criteria of Silverman et al and further into 2 (FDG-2) patterns.

RESULTS: Agreement among the 7 visual-statistical categories by at least 2 of the 3 readers occurred in >94% of cases for all groups: Alzheimer disease, mild cognitive impairment, and normal cognitive. Perfect matches by all 3 raters were observed for 62% of the cases by FDG-7 and 76 by FDG-2. Inter-rater concordance was moderate by FDG-7 ($\kappa = 0.57$) and substantial in FDG-2 ($\kappa = 0.67$) on average. The FDG-PET score, an automated quantitative index developed by Herholz et al, increased as the number of raters who voted for the AD pattern increased ($\rho = 0.59$, $P < .0001$), and the FDG-PET score decreased as those for normal pattern increased ($\rho = -0.64$, $P < .0001$).

CONCLUSIONS: Inter-rater agreement was moderate to substantial for the combined visual-statistical interpretation of ^{18}F-FDG-PET and was also significantly associated with automated quantitative assessment.

ABBREVIATIONS: AD = Alzheimer disease; J-ADNI = Japanese Alzheimer's Disease Neuroimaging Initiative; MCI = mild cognitive impairment; NC = cognitively normal subject

PET can visualize regional glucose metabolism by using ^{18}F-FDG; and hypometabolism in the posterior cingulate/precuneus and temporoparietal cortices is regarded as a typical uptake pattern of Alzheimer disease (AD).[1] These findings are considered useful for differentiating AD from other disorders presenting with dementia as well as for predicting conversion from mild cognitive impairment (MCI) to AD.[2,3]

Three approaches for evaluating brain PET images are visual interpretation alone, visual interpretation with adjunctive statis-

Received February 21, 2013; accepted after revision May 2.

From the Division of Molecular Imaging (T.Y., Y.I., T.N., M. Senda), Institute of Biomedical Research and Innovation, Kobe, Japan; Department of Radiology (Kazunari Ishii), Kinki University Faculty of Medicine, Osakasayama, Japan; Positron Medical Center (Kenji Ishii), Tokyo Metropolitan Institute of Gerontology, Tokyo, Japan; Department of Brain Science and Molecular Imaging (T.K., K. Ito), National Center for Geriatrics and Gerontology, Obu, Japan; David Geffen School of Medicine (D.H.S.S.), University of California, Los Angeles, Los Angeles, California; Department of Psychiatry (T.A.), University of Tsukuba, Tsukuba, Japan; Department of Geriatrics and Gerontology (H.A.), Tohoku University, Sendai, Japan; Institute of Brain and Blood Vessels (M. Sugishita), Isezaki, Japan; Department of Neuropathology and Neuroscience (T.I.), University of Tokyo, Tokyo, Japan; Research Association for Biotechnology (Y.I., T.N.), Tokyo, Japan; and J-ADNI Core (T.Y., Y.I., T.N., Kazunari Ishii, Kenji Ishii, T.K., Kengo Ito, M.S., T.A., H.A., M.S., T.I.).

The Research Group of the Japanese Alzheimer's Disease Neuroimaging Initiative comprised investigators from 38 different facilities. The investigators contributed to the design and implementation of J-ADNI and/or provided data but did not participate in the analyses of this report.

T. Yamane contributed to concept and design, analyzed data, and wrote the manuscript. Y. Ikari and T. Nishio acquired and analyzed PET data. Kazunari Ishii, Kenji Ishii, T. Kato, and K. Ito acquired and interpreted PET data. D.H.S. Silverman critically revised the manuscript and enhanced its intellectual content. M. Senda critically revised the manuscript, enhanced its intellectual content, and approved the final content of the manuscript. T. Asada, H. Arai, M. Sugishita, and T. Iwatsubo acquired clinical data and approved the final content of the manuscript.

This work is a part of the Translational Research Promotion Project/Research Project for the Development of a Systematic Method for the Assessment of Alzheimer's Disease, sponsored by the New Energy and Industrial Technology Development Organization of Japan. The Japanese Alzheimer's Disease Neuroimaging Initiative is also supported by a Grant-in-Aid for Comprehensive Research on Dementia from the Japanese Ministry of Health, Labour and Welfare, as well as by the grants from J-ADNI Pharmaceutical Industry Scientific Advisory Board companies.

Paper previously presented in part at: Annual Meeting of the Society of Nuclear Medicine, June 4–8, 2011; San Antonio, Texas.

Please address correspondence to Tomohiko Yamane, MD, PhD, Division of Molecular Imaging, Institute of Biomedical Research and Innovation, 2–2, Minatojima-minamimachi, Chuo-ku, Kobe, 650-0047, Japan; e-mail address: yamane@fbri.org

Indicates open access to non-subscribers at www.ajnr.org

Evidence-Based Medicine Level 2.

http://dx.doi.org/10.3174/ajnr.A3665